RSC Advances

PAPER

View Article Online
View Journal | View Issue

Cite this: *RSC Adv.*, 2023, **13**, 34107

Binding interactions of hydrophobically-modified flavonols with β-glucosidase: fluorescence spectroscopy and molecular modelling study

Liudmyla V. Chepeleva,[a] Oleksii O. Demidov,[a] Arsenii D. Snizhko,[a] Dmytro O. Tarasenko,[a] Andrii Y. Chumak,[a] Oleksii O. Kolomoitsev,[a] Volodymyr M. Kotliar,[a] Eugene S. Gladkov,[ab] Alexander Kyrychenko *[ab] and Alexander D. Roshal[a]

Natural flavonoids are capable of inhibiting glucosidase activity, so they can be used for treating diabetes mellitus and hypertension. However, molecular-level details of their interactions with glucosidase enzymes remain poorly understood. This paper describes the synthesis and spectral characterization of a series of fluorescent flavonols and their interaction with the β-glucosidase enzyme. To tune flavonol–enzyme interaction modes and affinity, we introduced different polar halogen-containing groups or bulky aromatic/alkyl substituents in the peripheral 2-aryl ring of a flavonol moiety. Using fluorescence spectroscopy methods in combination with molecular docking and molecular dynamics simulations, we examined the binding affinity and identified probe binding patterns, which are critical for steric blockage of the key catalytic residues of the enzyme. Using a fluorescent assay, we demonstrated that the binding of flavonol **2e** to β-glucosidase decreased its enzymatic activity up to 3.5 times. In addition, our molecular docking and all-atom molecular dynamics simulations suggest that the probe binding is driven by hydrophobic interactions with aromatic Trp and Tyr residues within the catalytic glycone binding pockets of β-glucosidase. Our study provides a new insight into structure–property relations for flavonol–protein interactions, which govern their enzyme binding, and outlines a framework for a rational design of new flavonol-based potent inhibitors for β-glucosidases.

Received 14th September 2023
Accepted 13th November 2023

DOI: 10.1039/d3ra06276g

rsc.li/rsc-advances

Introduction

Flavonol-based fluorescent probes represent a class of environmentally sensitive dyes whose emission properties are highly sensitive to their immediate environment.[1–7] The notable feature of these probes is that due to the presence of a hydroxyl group at the 3-position of a flavonoid moiety, they are capable of excited-state intramolecular proton transfer (ESIPT) (Scheme 1). A proton transfer reaction occurs through an intramolecular hydrogen bond bridge, resulting in an extremely fast ($k_{ESIPT} > 10^{12}$ s^{-1}) phototautomerization from the normal state (N*) to the tautomer state (T*).[7–9] ESIPT leads to the appearance of dual-wavelength emission in flavonols. An essential advantage of ESIPT probes is that an intensity ratio of their normal-to-tautomer emission bands can be tuned by electron donor/acceptor substituents in a flavonol moiety.

The emission life time and quantum yield of flavonols depends strongly on the environment properties.[1,8,10] Flavonol-based probes have been utilized as environment-sensitive fluorophores for monitoring solvent polarity[1,11,12] and pH,[13,14] as well as the determination of water traces in organic solvents.[15] The unique optical properties and biocompatibility make flavonols a promising fluorescence probe for studying the

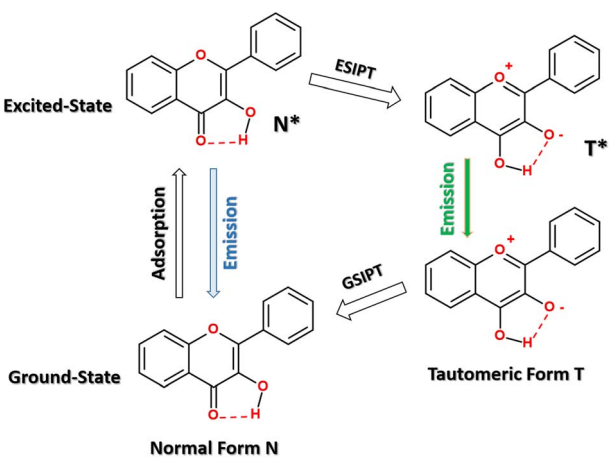

Scheme 1 Scheme of an excited-state intramolecular proton transfer (ESIPT) in flavonol.

[a]*Institute of Chemistry, V.N. Karazin Kharkiv National University, 4 Svobody Sq., Kharkiv 61022, Ukraine. E-mail: a.v.kyrychenko@karazin.ua*

[b]*State Scientific Institution "Institute for Single Crystals", National Academy of Sciences of Ukraine, 60 Nauky Ave., Kharkiv 61072, Ukraine*

structure of amphiphilic polymers[16] and biomacromolecules.[17] A large fluorescence "turn-on" effect has been observed upon selective binding of flavonols to some proteins, such as lysozymes[18] and albumins.[17,19] The selectivity of flavonols for certain proteins has been utilized for developing new fluorescence detection assays.[17,20,21] Moreover, flavonol-based probes have also demonstrated a low perturbation impact on the lipid membrane physical state,[22] so some fluorescent flavonols were utilized for fluorescent cell imaging.[23–25]

It has recently been demonstrated that flavonol-based probes, such as 4′-fluoroflavonol β-D-glucopyranoside, could be used as a fluorescent indicator of β-glucosidase activity.[26,27] β-Glucosidases are a family of hydrolase enzymes that catalyze the hydrolysis of aryl and alkyl β-D-glucosides and cellobioses. β-Glucosidases are present in plants, fungi, animals, and bacteria. In addition, these enzymes are promising reagents in various biotechnological processes because they can catalyze the hydrolysis of many artificial substrates upon biofuel production and oligosaccharide cleavage.[28] Regulation of glucosidase activity plays a key role in treating Gaucher's disease[29] and the effectiveness of chemotherapy for breast cancer.[30] Therefore, many glycosidase inhibitors have been isolated from natural sources or synthesized to optimize their inhibitory potency.[31–37] Inhibition of the catalytic activity of glycosidase enzymes has great potential in developing highly potent and specific drugs against such diseases as diabetes, cancer, and viral infections.[37,38]

In this work, we studied the binding interaction of a series of synthetic flavonols with a β-glucosidase enzyme using fluorescence titration measurements and computational chemistry tools, such as molecular docking and molecular dynamics simulations. A series of flavonol derivatives was designed by varying different substituents in the peripheral 2-aryl moiety. The fluorescence titration of the flavonols with β-glucosidase in aqueous solution revealed pronounced protein-induced fluorescence "turn-on" effects, which are characteristic for the probe binding to the hydrophobic water-free cavity of the protein. In addition, the favorable binding mode of the flavonols into β-glucosidase enzymes taken from different sources was identified by molecular docking calculations. Finally, the stability of the docked flavonol–enzyme complexes was further re-examined by all-atom molecular dynamics simulations in an explicit water solution.

Experimental section

Chemistry

Synthesis of flavonols 2a–f. The synthesis of 2-aryl-3-hydroxy-4*H*-chromen-4-ones (3-hydroxyflavones or flavonols) was carried out by Scheme 2.

2-Aryl-3-hydroxy-4*H*-chromen-4-ones **2a–f** were synthesized by the following method. For the synthesis of the target 2-aryl-3-hydroxy-4*H*-chromen-4-ones **2a–f**, we used the one-pot optimized method[27] without obtaining and additional purification of the corresponding intermediate unsaturated ketones. The synthesis of unsaturated ketones **1a–f** described elsewhere.[39] The general procedures of the synthesis of most typical substances of the series used in our work and typical examples

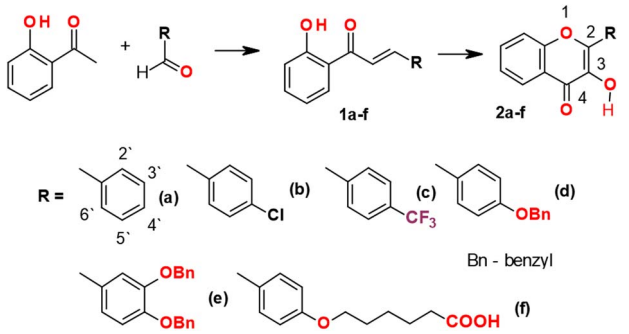

Scheme 2 Chemical structure and preparation of flavonols **2a–f**.

of substance characteristics are given in the experimental section.

General procedures for the preparation of substituted 3-hydroxy-2-(phenyl)-4*H*-chromen-4-ones (2a–f). 1.36 g (10 mmol) of 2-hydroxyacetophenone and corresponding benzaldehyde (10 mmol) were dissolved in methanol (50 mL) and solution of 3.36 g (60 mmol) potassium hydroxide in water (10 mL) was added to the reaction mixture at stirring. The mixture was stirred at RT for 12 hours and monitored with TLC (solvent 1 : 1 $CHCl_3$: *n*-hexane). 3.4 mL (30 mmol) 30% H_2O_2 was added dropwise to the mixture. After 30 min mixture was acidified with 10% HCl to pH 3. The obtained precipitate was filtered off and washed by water and *n*-hexane. The crud product was re-crystalized from the corresponding solvents.

*2-Phenyl-3-hydroxy-4H-chromen-4-one (**2a**).* Yield 1.92 g (81%), mp 170.0–172.0 °C (ethanol). ^{1}H NMR (400 MHz, DMSO-d_6), δ, ppm: 9.65 (s), 8.23 (d, J = 7.40 Hz, 2H), 8.13 (dd, J = 8.04, 1.12 Hz, 1H), 7.82–7.76 (m, 2H), 7.60–7.56 (m, 2H), 7.53–7.46 (m, 2H). ^{13}C NMR (126 MHz, DMSO-d_6), δ, ppm: 173.0, 154.6, 145.2, 139.1, 133.7, 131.3, 129.9, 128.5, 127.6, 124.8, 124.5, 121.3, 118.4. Mass spectrum, m/z (I_{rel}, %): 239 $[M + H]^+$ (100). Found, %: C 75.67; H 4.18. $C_{15}H_{10}O_3$. Calculated, %: C 75.62; H 4.23. These data are in accordance with the literature.[27]

*2-(4-Chlorophenyl)-3-hydroxy-4H-chromen-4-one (**2b**).* Yield 1.45 g (53%), beige crystals, mp 201.0–201.5 °C (ethanol). ^{1}H NMR (400 MHz, DMSO-d_6), δ, ppm: 9.8 (bs, 1H, OH), 8.25 (d, J = 8.4 Hz, 2H), 8.12 (d, J = 8.1 Hz, 1H), 7.82 (dd, 1H), 7.78 (t, 1H), 7.65 (d, J = 8.4 Hz, 2H), 7.48 (t, 1H). ^{13}C NMR (126 MHz, DMSO-d_6), δ, ppm: 172.9, 154.4, 143.9, 139.3, 134.4, 133.8, 130.1, 129.2, 128.6, 124.7, 124.5, 121.2, 118.3. Mass spectrum, m/z (I_{rel}, %): 157.0 (31), 273.0 $[M + H]^+$ (100), 275.0 (25). Found, %: C 66.11; H 3.29. $C_{15}H_9ClO_3$. Calculated, %: C 66.07; H 3.33. These data are in accordance with the literature.[40]

*2-(4-(Trifluoromethyl)phenyl)-3-hydroxy-4H-chromen-4-one (**2c**).* Yield 1.89 g (62%), beige crystals, mp 186.5–187.0 °C (ethanol). ^{1}H NMR (400 MHz, DMSO-d_6), δ, ppm: 10.0 (bs, 1H, OH), 8.35 (d, J = 8.4 Hz, 2H), 8.06 (d, J = 8.1 Hz, 1H), 7.83 (d, J = 8.4 Hz, 2H), 7.74 (dd, 1H), 7.67 (d, 1H), 7.42 (t, 1H). ^{13}C NMR (126 MHz, DMSO-d_6), δ, ppm: 173.5, 154.9, 143.5, 140.6, 135.6, 134.4, 128.5, 125.7, 125.6, 125.3, 125.0, 121.7, 118.8. Mass spectrum, m/z (I_{rel}, %): 58.5 (27), 307.2 $[M + H]^+$ (100). Found, %: C 62.69; H 2.91. $C_{16}H_9F_3O_3$. Calculated, %: C 62.75; H 2.96. These data are in accordance with the literature.[27]

2-(4-Benzyloxyphenyl)-3-hydroxy-4H-chromen-4-one (**2d**). Yield 2.92 g (85%), yellowish crystals, mp 175.0–176.0 °C (ethanol). ^{1}H NMR (400 MHz, DMSO-d_6), δ, ppm: 9.45 (s, 1H), 8.24–8.17 (m, 3H), 8.11 (dd, J = 8.0, 1.6 Hz, 1H), 7.83–7.71 (m, 3H), 7.53–7.30 (m, 8H), 7.21 (dd, J = 8.6, 1.6 Hz, 3H), 5.21 (s, 2H). ^{13}C NMR (126 MHz, DMSO-d_6), δ, ppm: 173.1, 159.9, 154.9, 145.9, 138.7, 137.1, 133.9, 129.8, 128.9, 128.4, 128.3, 125.2, 124.9, 124.2, 121.8, 118.8, 115.3, 69.8. Mass spectrum, m/z (I_{rel}, %): 345 $[M + H]^+$ (100). Found, %: C 76.69; H 4.70. $C_{22}H_{16}O_4$. Calculated, %: C 76.73; H 4.68. These data are in accordance with the literature.[41]

2-(3,4-Dibenzyloxyphenyl)-3-hydroxy-4H-chromen-4-one (**2e**). Yield 3.92 g (87%), pale yellow crystals, mp 145.0–146.0 °C (ethanol). ^{1}H NMR (400 MHz, DMSO-d_6), δ, ppm: 9.48 (s, 1H), 8.10 (d, J = 7.9 Hz, 1H), 7.96–7.91 (m, 1H), 7.91–7.85 (m, 1H), 7.83–7.71 (m, 2H), 7.61–7.16 (m, 12H), 5.23 (d, J = 9.4 Hz, 4H). ^{13}C NMR (126 MHz, DMSO-d_6), δ, ppm: 173.1, 154.8, 150.2, 148.2, 145.7, 138.8, 137.5, 137.3, 134.0, 128.9, 128.4, 128.3, 128.1, 125.2, 124.9, 124.4, 122.4, 121.7, 118.8, 114.2, 70.9, 70.3, 60.2. Mass spectrum, m/z (I_{rel}, %): 451 $[M + H]^+$ (100). Found, %: C 77.36; H 4.88. $C_{29}H_{22}O_5$. Calculated, %: C 77.32; H 4.92. These data are in accordance with the literature.[42]

6-(4-(3-Hydroxy-4-oxo-4H-chromen-2-yl)phenoxy)hexanoic acid (**2f**). Yield 1.66 g (45%), yellow solid, mp 185.5–186.0 °C (ethanol : DMF 3 : 1). ^{1}H NMR (400 MHz, DMSO-d_6), δ, ppm: 12.0 (bs, 1H, COOH), 10.5 (bs, 1H, OH), 8.23–8.16 (m, 2H, Ar), 8.09 (d, 1H, Ar), 7.75 (d, 2H, Ar), 7.44 (t, 1H, Ar), 7.10 (d, 2H, Ar), 4.06–4.16 (m, 2H, CH_2), 2.26–2.19 (m, 2H, CH_2), 1.76–1.71 (m, 2H, CH_2), 1.60–1.52 (m, 2H, CH_2), 1.46–1.40 (m, 2H, CH_2). ^{13}C NMR (126 MHz, DMSO-d_6), δ, ppm: 179.8, 159.6, 158.8, 143.3, 138.7, 134.6, 130.0, 129.4, 128.6, 123.6, 119.7, 119.2, 72.8, 38.9, 33.6, 30.3, 29.5. Mass spectrum, m/z (I_{rel}, %): 157.0 (12), 369.2 $[M + H]^+$ (100). Found, %: C 68.42; H 5.50. $C_{21}H_{20}O_6$. Calculated, %: C 68.47; H 5.47.

Materials and methods

^{1}H and ^{13}C NMR spectra (400 and 100 MHz) were recorded on Bruker Avance 400 and Varian MR-400 spectrometers in DMSO-d_6. ^{1}H and ^{13}C chemical shifts were reported relative to residual protons and the carbon atoms of the solvent (2.49 and 39.5 ppm, respectively) as the internal standard. The LCMS spectra were recorded using a chromatography/mass spectrometric system that consists of a high-performance liquid chromatography Agilent 1100 Series equipped with a diode matrix and a mass selective detector Agilent LC/MSD SL, column SUPELCO Ascentis Express C18 2.7 μm 4.6 mm × 15 cm. Elemental analysis was realized on a EuroVector EA-3000 instrument. TLC was performed using Polychrom SI F254 plates. Melting points of all synthesized compounds were determined with a Hanon Instruments automatic melting point apparatus MP450 in open capillary tubes.

According to the HPLC MS data, all synthesized compounds are >95% pure. All solvents and reagents were commercial grade and, if required, purified in accordance with the standard procedures. Starting unsaturated ketones were synthesized as described in ref. 43.

β-Glucosidase enzyme (β-D-glucoside glucohydrolase) from almonds were purchased as lyophilized powder with >98% purity from Sigma-Aldrich.

Spectroscopic measurements

UV-vis absorption spectra were measured using Agilent Cary 3500 UV-Vis Multicell Spectrophotometer. Fluorescence spectra were recorded using a Hitachi 850 steady-state fluorescence spectrometer equipped with double-grating excitation and emission monochromators. The fluorescence measurements were made in the neutral aqueous solution in a 10 × 10 mm cuvette maintained at 20 °C.

Fluorescence assay for β-glucosidase activity

β-Glucosidase enzymatic activity was tested using a fluorescent indicator based on flavonol β-D-glucoside. The fluorescence assay principle relies on the enzymatic cleavage (hydrolysis) of a glycosidic bond of a weakly fluorescent indicator, which results in the release of a brightly fluorescent flavonol aglycone fluorophore that is readily extracted by an organic phase. The details of this assay and its working principles have recently been described in detail elsewhere.[26,27]

In brief, a stock solution of a flavonol β-D-glucoside was prepared by dissolving its small aliquot in DMSO. A stock solution of β-glucosidase from almond was prepared by dissolving an enzyme in an aqueous phosphate buffer with pH = 6.86. Next, both aliquots were transferred to 1 mL of a buffer solution (pH = 6.86) and were used for kinetic studies of enzymatic cleavage. Concentrations of a flavonol β-D-glucoside indicator and β-glucosidase enzyme ranged from 5.0 to 7.0 × 10^{-5} mol L^{-1}.

The enzymatic hydrolysis reaction was carried out while stirring the mixture at a constant temperature. During the hydrolysis process, after reaction initialization, aliquots of 0.1 mL were taken at 1, 2, 6, 10, 15, and 30 min. Immediately after sampling, each aliquot was transferred to 2.5 mL of dichloromethane and intensively shaken. Using extraction, a mixture of the original flavonol β-D-glucoside and its hydrolyzed derivative – a flavonol aglycone, were separated from the enzyme. Next, the fluorescence spectra of the mixture of the flavonol β-D-glucoside and the corresponding aglycone were recorded in the organic phase.

The fluorescence was excited at 360 nm and the fluorescence spectra were recorded in the range of 380–600 nm using a Hitachi 850 spectrofluorimeter. The emission intensity (I_A) at the maximum of the long-wavelength fluorescence band at 525 nm was used for quantitative kinetics studies. The value of I_A, which is proportional to the aglycone concentration and inversely proportional to the glucoside concentration, was used to determine the reaction order and calculate the rate constant of the enzymatic hydrolysis.

Molecular docking setup

The molecular docking setting up, addition of hydrogen, the calculation of the Gasteiger charges of the receptor and ligands were performed using the AutoDock Tools (ADT) software,

version 1.5.7.[44] Molecular docking calculations were performed with the AutoDock Vina 1.1.2 software.[45] The 3D X-ray structure of *Paenibacillus polymyxa* β-glucosidase B (BglB, PDB ID: 2O9R),[46] *Raucaffricine* β-glucosidase (*r*BG, PDB ID: 4A3Y),[47] *Thermogota maritima* β-glucosidase (*Tm*GH1, PDB ID: 1OD0),[48] and human cytosolic β-glucosidase (hCBG, PDB ID: 2JFE)[49] were downloaded from the RCSB Protein Data Bank.

Ligand–protein interactions were studied by the semi-flexible molecular docking, so that the receptor was kept rigid and the ligand molecules were conformational flexible. The docking details of glucosidases are summarized in Table 1. Docking cell size was 45 × 45 × 45 and the grid point spacing set to 0.375 Å, respectively. For all runs, the number of binding modes was set to 9 and the exhaustiveness to 256. For each ligand, three independent runs were performed using different random seeds. The best docking mode corresponds to the largest ligand-binding affinity.

Molecular dynamic simulations

The X-ray structure of β-glucosidase was obtained from the Protein Data Bank. Co-crystalized ligands and water molecules were removed from the X-ray data. Protonation states for all titratable residues were set at their default state at pH = 7. The molecular topology of a protein was built by using pdb2gmx GROMACS tool. LigParGen web-server was used to generate the molecular topology for flavonols.[50,51] The OPLS-AA force field was used for the proteins and the flavonols.[52] TIP3P model[53] was used to treat explicit water molecules.

An initial structure of a probe–protein complex was taken from the corresponding most favourable structure obtained by the molecular docking calculations. The complex was solvated in cubic cell with a size of 9 nm. The system was first pre-equilibrated at NVT ensemble for 2 ns, during which probe and protein structure was positionally restrained. Second, the free unconstrained equilibration of a probe–protein complex was carried out for 0.1 ns at an NPT ensemble, during which a MD box cell size was allowed to relax. The final equilibrated configuration of the system was used to sample productive MD simulations for 200 ns.

All productive MD simulations were carried out for an NPT ensemble. The reference temperature of 298.15 K was kept constant using the v-rescale weak coupling scheme[54] with the coupling constant $\tau_T = 0.1$ ps. The constant pressure of 1 atm was maintained using the Parrinello–Rahman barostat with the coupling constant $\tau_P = 1$ ps. The initial atomic velocities were generated with a Maxwellian distribution at the given absolute temperature. Periodic boundary conditions were applied to all three directions of the simulated box. Electrostatic interactions were simulated with the particle mesh Ewald (PME) approach[55] using the long-range cut-off of 1.1 nm. The cut-off distance of Lennard–Jones interactions was also equal to 1.1 nm. The MD simulation time step was 2 fs with the neighbour list updates every 10 fs. All bond lengths were kept constant using the LINCS routine.[56,57] The MD simulations were carried out using the GROMACS set of programs, version 2019.4.[58]

Molecular graphics and visualization were performed using VMD 1.9.3.[59]

Table 1 The catalytic Glu residues and Cartesian coordinates of a docking cell center for studied β-glucosidases from four different sources

Enzyme, PDB code	Catalytic residues	Cartesian coordinates of docking cell center, (x, y, z)
BglB, 2O9R	Glu167, Glu356	67.1, 31.2, 38.8
rBG, 4A3Y	Glu186, Glu420	16.8, 23.9, 41.6
TmGH1, 1OD0	Glu166, Glu351	0.0, 13.1, 12.7
hCBG, 2JFE	Glu165, Glu373	38.8, 53.2, 36.7

Results and discussion

Spectral properties of flavonols 2a–f

The optical properties of flavonol derivatives have been examined in various solvents.[4,11,60] A numerous studies demonstrated that their fluorescence properties are essentially dependent on the environment, so that upon going from non-polar solvents, such as hexane, to polar protic water solution, their fluorescence quantum yield decreases significantly from 0.4 up to 0.02, respectively.[10,11,26,27] Table 2 summarizes the spectral properties of flavonols **2a–f** in water. A key feature of emission of **2a–f** is a high Stokes shift of their long-wavelength band varying from 8100 up to 9925 cm^{-1}, which originates from the ESIPT tautomer.

Fluorescence studying protein–flavonol binding interaction

Fluorescence properties of flavonols **2a–f** were studied in aqueous neutral solution in the presence and the absence of β-glucosidase (Fig. 1). Despite the wide use of flavonols in biomedical applications, their solubility in water is known to be very low, being about (0.12, 0.5, and <0.01) g L^{-1} at 20 °C for rutin, naringin, and quercetin, respectively.[61,62] Therefore, the flavonols were added into the solution as a small aliquot of their DMSO stocks. Next, to study flavonol–enzyme binding interaction, we utilized fluorescence titration protocol, in which the concentration of flavonols in water solution was fixed at ~1–2 × 10^{-5} M and the concentration of glucosidase was varied in a range from 0 up to 7 × 10^{-4} M, respectively.

Fluorescence titration experiments and emission spectra of flavonol **2a–f** in the aqueous solution are summarized in Fig. 1. As can be seen, significant fluorescence changes, such as fluorescence enhancement and the appearance of new emission bands, were observed for flavonol **2a–f** upon titration with β-glucosidase stocks. The increase in the fluorescence intensity of an environment-sensitive probe is known as the protein-induced "turn-on" effect. The observed spectral changes of flavonols **2a–f** are indicative of changes in the local environment around the probe. Upon binding to the protein, a flavonol probe leaves a polar aqueous solution and penetrates a nonpolar hydrophobic environment inside a protein pocket. The fluorescence increase is associated with the loss of water-induced fluorescence quenching of **2a–f**, which

Table 2 Absorption and fluorescence parameters of flavonols **2a–f** in water

Flavonol	Absorption maximum, nm	Fluorescence maximum (normal/tautomer), nm	Fluorescence Stokes shift, cm^{-1}
2a	343	520	9925
2b	366	540	8800
2c	355	540	9650
2d	362	445/540	5150/9100
2e	379	443/547	3810/8100
2f	356	445/542	5620/9640

might be due to deep penetration of the flavonols into the hydrophobic, water-free region of the β-glucosidase enzyme pocket.

The detailed analysis of spectral changes in the studied flavonols demonstrates that the titration of **2a** was mainly accompanied by the increase in the emission of the tautomer band at 545 nm (Fig. 1A). In contrast, more complex spectral changes were observed for the cases of substituted flavonols **2b–f**. These changes included the redistribution of normal-to-tautomer intensity at 440/545 nm and the appearance of the new band at 514 nm (Fig. 1B–F). Measuring the emission spectrum at pH > 10 allowed us to assign that the new emission band at 514 nm belongs to an anionic form (A) of a flavonol (Fig. 2).

The appearance of acid–base equilibrium in flavonols (Fig. 2A) has been observed for its other derivatives in aqueous and non-aqueous polar protic solvents.[9–11]

The quantitative interpretation of protein–ligand interactions can be analysed using site-specific or nonspecific binding models, such as Michaelis–Menten, Hill or Scatchard formalisms.[63–66] Taking into account that the binding behaviour of numerous ligands to enzymes of a glucosidase family has been well-characterized and, in most cases, demonstrated the single-site specific binding to the primary catalytic pocket,[67–71] we first considered "one site-specific binding" model.[63]

Relative fluorescence intensities of flavonol **2a–f** were plotted as a function of the concentration of β-glucosidase, as shown in Fig. 3.

First, the fluorescence titration data were analyzed using nonlinear regression with "one site-specific binding" model by eqn (1):

$$I_i = \frac{I_{max} C_g}{K_d + C_g} \quad (1)$$

where C_g is the concentration of β-glucosidase, I_i is the apparent fluorescence intensity, I_{max} is the fluorescence maximum at the complete binding and K_d is the equilibrium dissociation constant.

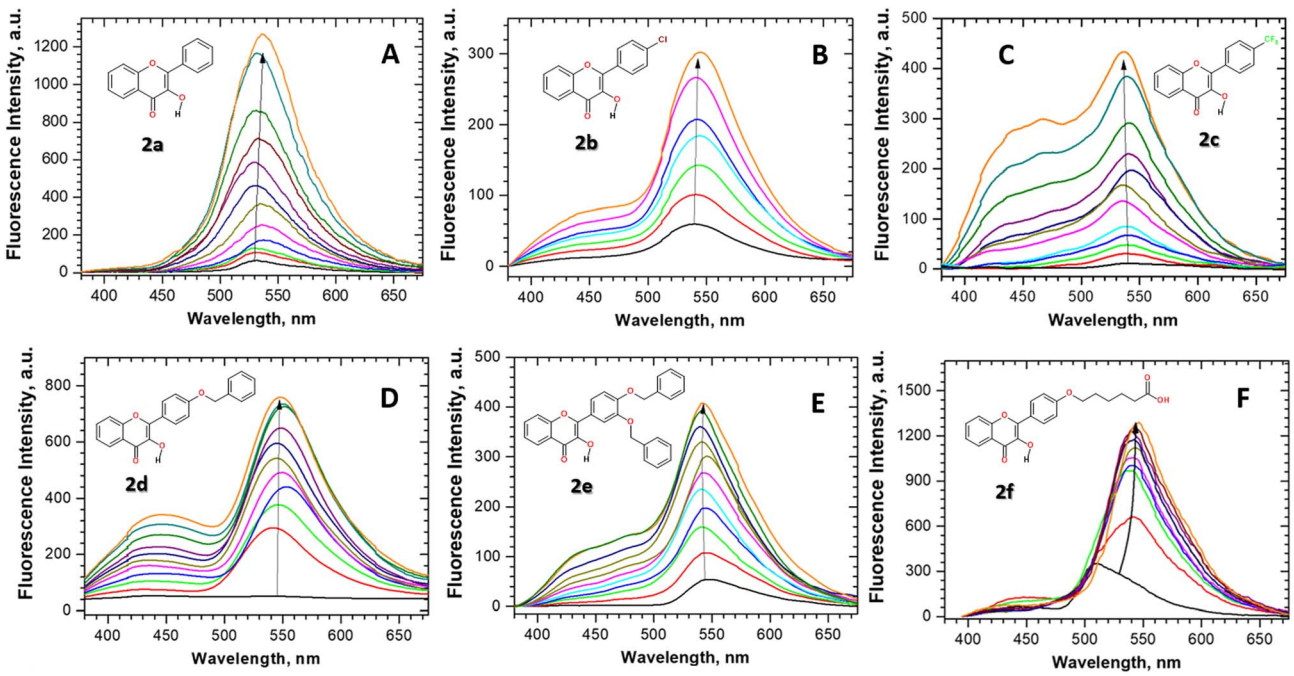

Fig. 1 (A–F) Fluorescence titration of flavonols **2a–f** with β-glucosidase in the neutral aqueous solution at 298 K. The fluorescence was excited at 360 nm. The arrow corresponds to increase in the fluorescence intensity of the flavonols upon the increase in β-glucosidase concentration. In the typical titration experiment, the flavonol concentration was kept fixed at ~1–2 × 10^{-5} M, whereas the β-glucosidase concentration was varied in a range from 0.5 × 10^{-5} up to 7 × 10^{-4} M, respectively.

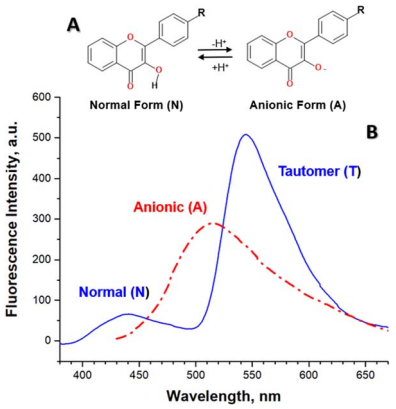

Fig. 2 (A) Scheme of acid–base equilibrium in flavonols in an aqueous solution. (B) The fluorescence spectra of flavonol **2d** in the neutral (excitation at 360 nm, solid blue) and the base aqueous solution (excitation at 420 nm, dash-dotted red).

The binding constant of ligand–protein interaction can be expressed by eqn (2).

$$K_b = \frac{1}{K_d} \quad (2)$$

Fig. 3A shows the titration data were well fitted by "one site-specific binding" model using eqn (1). From these data, the binding constant K_b for flavonol–enzyme interaction was summarized in Table 3.

As seen from Table 3, introducing substituents 4′-Cl and 4′-CF_3 into a flavonol moiety has little effect on the binding constant of flavonols **2b** and **2c**, respectively. Surprisingly, small changes in the binding constant were also observed after introducing the bulk 4′-*O*-benzyl group in flavonol **2d**. However, a significant increase in the binding rate was found for flavonols **2e** and **2f**, bearing large and bulky 3′,4,′-dibenzyloxy and 4′-hexylcarboxylic fragments (Table 3). These findings suggest that in the studied series, the binding interaction with β-glucosidase was mainly driven by van-der-Waals interactions and hydrophobic forces.

Considering the critical role of hydrophobic forces in the flavonol–enzyme binding, the interactions between a flavonol probe and the enzyme can alternatively be regarded as probe partitioning from the aqueous solution into the hydrophobic region of the protein. Therefore, we re-analyzed our titration experiments by using partitioning formalism.

The apparent partition coefficient K_p was determined by fitting fluorescence intensities, I_i, measured at the fixed wavelength 540 nm, to eqn (3):

$$I_i = I_0 + \frac{I_{max} C_g}{[W] + K_p C_g} \quad (3)$$

where I_{max} = the maximal fluorescence increase observed upon the complete partition, C_g is the molar concentration of β-glucosidase, [W] is the molar concentration of water (55.3 M), K_p is the mole fraction partition coefficient.[40] The Gibbs free energy ΔG of flavonol transfer from water to a protein environment was

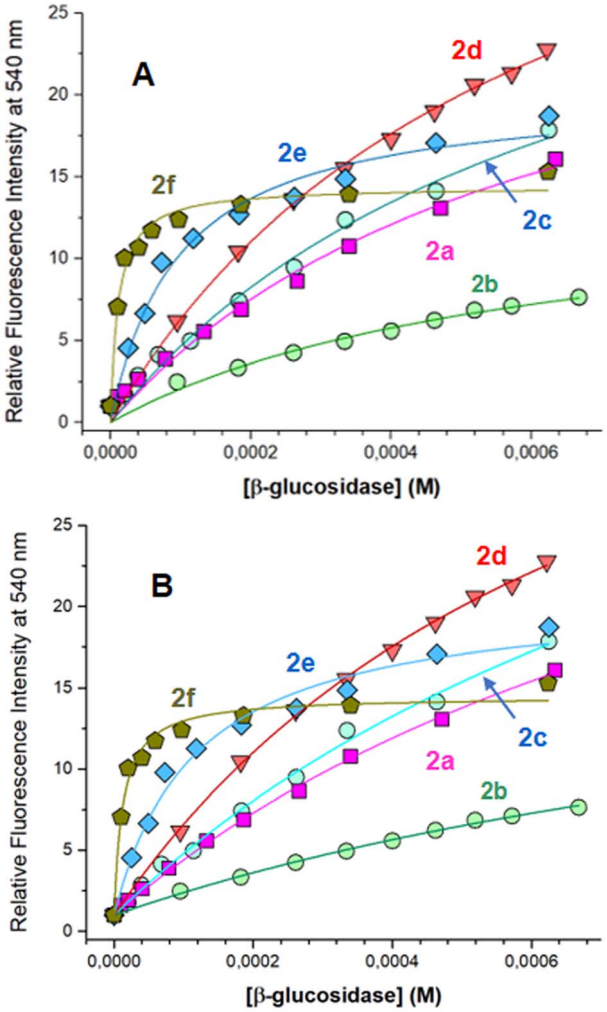

Fig. 3 Relative fluorescence intensities of flavonol **2a–f** in aqueous solution are plotted as a function of the concentration of β-glucosidase. Relative intensities (I_i/I_0, I_i is the apparent fluorescence intensity in the presence of β-glucosidase, and I_0 is the intensity in the solution with no β-glucosidase) were determined at fixed wavelengths of 540 nm. Titration profiles were fitted to eqn (1) (A) and eqn (3) (B) to determine the binding parameters, as summarized in Tables 3 and 4.

calculated from the mole fraction partition coefficients K_p using eqn (4):

$$\Delta G = -RT \ln K_p \quad (4)$$

where R is the gas constant and T is the absolute temperature. K_p and ΔG of flavonol partitioning in the protein pocket are summarized in Table 4.

Fig. 3B shows the analysis of the fluorescence titration data by a "partitioning" model using eqn (3). As can be seen, the titration data were well fitted by eqn (3). One can note that interactions of flavonols **2a–c** with β-glucosidase were characterized by the similar partitioning coefficient K_p (Table 4). Whereas flavonols **2e–f** favor the partitioning from water to the protein environment. The same trends are seen in the Gibbs free energy ΔG of partitioning, so that flavonols **2a–d** are

Table 3 The binding constants of flavonols **2a–f** with β-glucosidase estimated by eqn (1)

Flavonol	I_{max}	Binding constant K_b, mM
2a	30.9	1.61×10^3
2b	14.4	1.69×10^3
2c	36.3	1.47×10^3
2d	43.9	1.67×10^3
2e	20.2	1.04×10^4
2f	14.4	1.01×10^5

characterized with ΔG from −6.3 to −6.6 kcal mol^{-1}, whereas the essential increase ΔG up to −7.7 and −9.1 kcal mol^{-1} observed for **2e** and **2f** (Table 4), respectively.

Protein homology in β-glucosidase family

Because the high-resolution 3D structure of commercial almonds β-glucosidase used in our experimental studies is currently unavailable, we first considered the available X-ray glucosidase structures from other sources. β-Glucosidase family includes enzymes with different activities widely distributed among all sorts of living organisms, which are capable of the common ability to hydrolyze β-glucosidic linkages of disaccharides, oligosaccharides or conjugated saccharides.[72] Among the members of this family are bacterial and fungal cellobiases that play an essential role in cellulolytic hydrolysis.[73]

Therefore, to carry out molecular docking analysis of flavonol–glucosidase interactions, we used β-glucosidase enzymes taken from various sources, such as *Paenibacillus polymyxa* β-glucosidase B (BglB), *Raucaffricine* β-glucosidase (*r*BG), *Thermogota maritima* β-glucosidase (*Tm*GH1) and human cytosolic β-glucosidase (hCBG), respectively. Despite the difference in amino acid residues around their glycone binding pockets, the sequence alignment of these enzymes revealed a high identity of above 90%, which is characteristic of the many members of this family.[46,49,73,74]

Fig. 4 shows the structure overlap of three different β-glucosidases. Despite some structure variations seen at peripheral protein regions, all enzymes are characterized by main common features: (i) they have a deep hydrophobic pocket capable of accommodating substrate molecules during cellulolytic hydrolysis (Fig. 4). (ii) The catalytic active site is composed of two glutamate (Glu) residues placed in close proximity to one another (Fig. 4). The 3D structure of BlgB, TmGH1, rBG, and hCBG glucosidases is well-resolved, so that these structures have already been used as a receptor model for molecular docking calculations.[75–79]

Table 4 The binding parameters of flavonols **2a–f** with β-glucosidase estimated by eqn (3)

Flavonol	I_{max}	Partitioning coefficient, K_p	ΔG, kcal mol^{-1a}
2a	40.6	5.07×10^4	−6.4
2b	20.9	3.96×10^4	−6.3
2c	46.9	4.91×10^4	−6.4
2d	47.3	7.47×10^4	−6.6
2e	19.8	4.78×10^5	−7.7
2f	13.5	4.39×10^6	−9.1

[a] Calculated at 298 K.

Molecular docking of flavonols against β-glucosidase

The structural and energetic parameters of flavonol interactions with β-glucosidases were examined using four different protein structures (Table 1). Molecular docking calculations demonstrate that all studied flavonols bind strongly and are able to insert deeply into a central cavity of β-glucosidase. Examples of binding modes of flavonols **2a–f** are shown for *Thermogota maritima* β-glucosidase (TmGH1) in Fig. 5 and 6. Molecular docking suggests that the binding affinity of **2a–f** towards β-glucosidase depends on the nature of peripheral substituents R and R_1 located in the 4′-aryl ring of the flavonols (Scheme 2). On the other hand, the choice of the β-glucosidase structure has little effect. Molecular docking results of flavonols **2a–f** with β-glucosidase from four different sources are summarized in Table 5.

One can note that, depending on the nature of the substitutions R and R_1, the binding affinity of flavonols **2a–f** varies in a range from −8.2 up to −9.6 kcal mol^{-1}. The etherification of the peripheral 3′ and 4′-hydroxyl groups in the 2-aryl moiety with the hydrophobic benzyl substituent significantly increases the affinity of the flavonols **2d–e** towards the β-glucosidase enzymes, so that the binding affinity of **2e** increases up to −11.7 kcal mol^{-1} (Table 5).

*Tm*GH1 enzyme has a deep hydrophobic pocket with an active site (about 16 Å deep) (Fig. 5 and 6). The two catalytic glutamate residues, the acid/base Glu166 and the nucleophile Glu352 are located deep within the active site. It can be seen that all studied flavonols **2a–f** bind close to the catalytic dyad Glu166–Glu351. The ligand binding is driven by hydrophobic interactions with aromatic Trp122, Trp168, Trp295, Trp324, Trp398, Trp406 as well as Tyr295, respectively. Moreover, the receptor-bound flavonols **2a–f** shield the active site residues Glu166 and Glu351 and restrict the accessibility of other

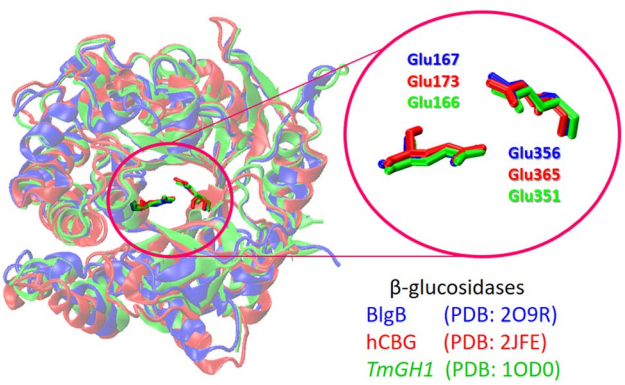

Fig. 4 Overlap of the protein structure and the conservative catalytic residues for β-glucosidases from different sources. The enzyme and the corresponding catalytic Glu residues are shown as color-coded sticks.

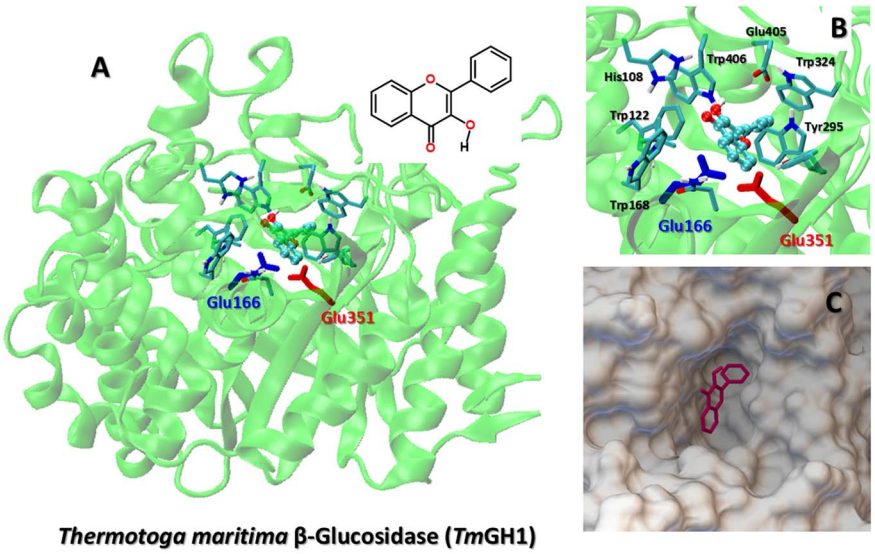

Fig. 5 (A) The best binding mode of flavonol **2a** to *Thermogota maritima* β-glucosidase (*Tm*GH1, PDB 1OD0). The catalytic residues Glu166 and Glu351 are shown as color-coded sticks. (B) The docking pose of flavonol **2a** in the enzyme pocket of *Tm*GH1. (C) The insert shows the binding mode of **2a** and key enzyme residues.

substrate molecules toward the catalytic center. Such a binding mode of **2a–f** holds promise of their high inhibitory potency against glucosidase activity.

It has been shown that the binding of bulk-size ligands into the glucosidase active site was able to inhibit the hydrolyze-type activity of these enzymes. The inhibition of α-glucosidases by natural flavonoids, such as combretol, morin,[80,81] myricetin,[68,81,82] ombuin, quercetin,[31,68,80,82] and retusin,[31] has been reported by using experimental and computational techniques. In addition, there are some reports that ligand binding within the enzyme cavity had complex multi-mode behavior, so that substrate binding occurred into different sub-sites of the β-glucosidase pocket.[83] Some studies reported that catalytic Glu residues did not interact with the scissile glycosidic bond of a ligand, indicating a shallow binding mode, where the substrate initially binds before moving into the active site. Such a mode has been reported for β-glucosidases in several GH families.[84] Moreover, it has been shown that the binding thermodynamics parameters of 1-deoxynojirimycin and isofagomine inhibitors towards almond β-glucosidase and *Thermogota maritima* β-glucosidase (*Tm*GH1) have similar values,[48] so despite the absence of the high-resolution X-ray structure of almond β-glucosidase, it can be well modeled by the corresponding *Tm*GH1 structure.

Therefore, we compared the molecular docking binding affinity of the studied flavonols **2a–f** with those of well-known inhibitors. For this purpose, we performed comparative re-docking of a series of structurally different inhibitors, summarized in Scheme 3. Compounds **Imd1** and **Imd2** are known to be among the most potent glycosidase inhibitors reported to date. It has been demonstrated that adding the hydrophobic phenethyl moiety in **Imd2** improves its binding by 20–80-fold, possibly due to significantly better entropic contributions to binding.[85]

It has been noticed that the peripheral phenyl rings of an inhibitor molecule could be faced towards the solvent-exposed region of an enzyme, which played an essential effect in anti-β-glucosidase activity.[34] Our molecular docking demonstrates that, in terms of the binding affinity, the studied flavonols are among strong β-glucosidase binders with the comparable and higher affinity than available inhibitors **Imd2** and **Cas2** (Table 5).

Determining β-glucosidase activity

To test if the strong binding affinity of the hydrophobically-modified flavonols, such as **2e** and **2f**, led to steric blockage of the enzymatic activity of β-glucosidase, we used flavonol-based fluorescent indicator – flavonol β-D-glucopyranoside **3** (Fig. 7).[26,27] The indicator has a β-D-glucopyranoside moiety attached to the 3-OH group of flavonol and it is characterized by weak emission. However, upon the enzymatic cleavage of the glycosidic bond, the indicator emission is essentially enhanced due to the appearance of bright aglycone fluorescence.[26]

The enzymatic activity of β-glucosidase was measured using a flavonol β-D-glucopyranoside indicator **3** in the absence and the presence of flavonol **2e**. The latter experiment was carried out by incubating β-glucosidase solution with flavonol **2e** for up to 1 h, followed by the enzymatic activity test.

The kinetic analysis of the enzymatic reaction demonstrated that, for the free β-glucosidase, the reaction rate constant k of the indicator hydrolysis was found to be 81.52 L mol^{-1} s^{-1} (Fig. 7). After the binding flavonol **2e** to β-glucosidase, re-measuring of the enzyme activity revealed that the rate constant k was decreased to 23.46 L mol^{-1} s^{-1}, indicating to a 3.5-time decrease in the enzymatic activity caused by flavonol **2e**.

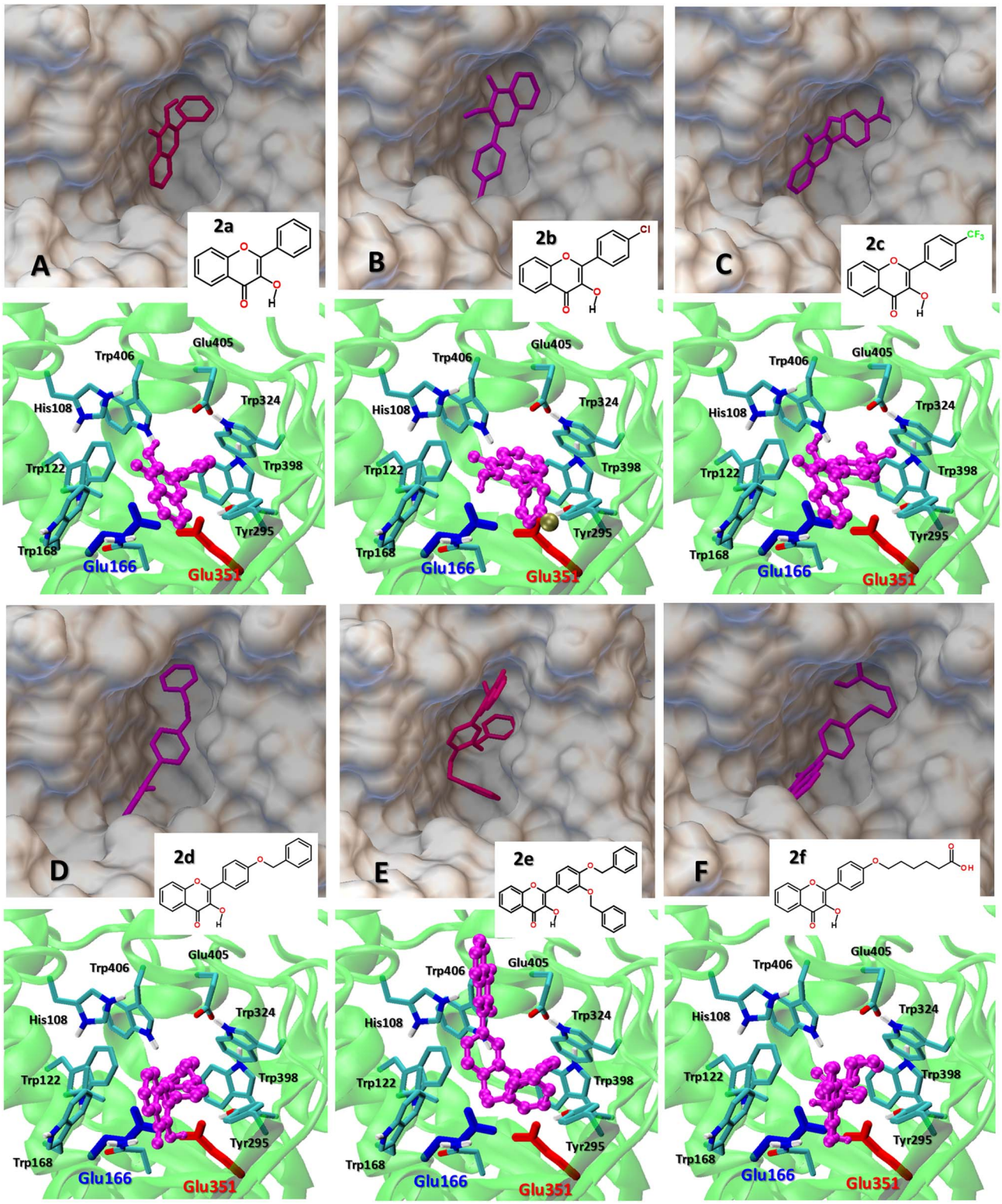

Fig. 6 (A–F) The comparison of the best binding mode of the studied flavonol **2a–f** at *Thermogota maritima* β-glucosidase (*Tm*GH1, PDB 1OD0). The catalytic residues Glu166 and Glu351 are shown as color-coded sticks. (Top) The insert shows the top view of the location of flavonols **2a–f** within the protein binding pocket. (Bottom) The side view of the flavonol–enzyme binding interaction within the active center region.

Molecular mechanism of flavonol–enzyme interactions

While molecular docking provides valuable information about the favorable binding mode and the ligand affinity towards an enzyme, its major drawback is the lack of explicit solvation effects. Therefore, the stability of the docking-derived flavonol–enzyme complexes in bulk water solution was further re-

Table 5 The binding affinity of flavonols **2a–f** and some known inhibitors towards β-glucosidases from various sources estimated by molecular docking calculations

	Binding affinity, kcal mol^{-1}			
	Human cytosolic β-Glucosidase	*Paenibacillus polymyxa* β-Glucosidase	*Thermotoga maritima* β-Glucosidase	*Raucaffricine* β-Glucosidase
Flavonol	(PDB: 2JFE)	(PDB: 2O9R)	(PDB: 1OD0)	(PDB: 4A3Y)
Studied flavonols				
2a	−8.8	−8.2	−8.5	−8.8
2b	−9.0	−8.4	−8.3	−8.6
2c	−9.8	−9.1	−9.2	−9.6
2d	−10.4	−9.0	−9.3	−9.3
2e	−11.6	−11.1	−11.0	−9.6
2f	−8.7	−9.1	−9.5	−8.7
Known inhibitors				
Noeuromycin	−6.1	−6.8	−6.3	−6.8
Isofagomine	−5.7	−6.0	−5.5	−5.8
Cas1	−7.4	−7.7	−7.8	−7.5
Cas2	−7.0	−7.7	−7.6	−7.4
Imd1	−5.8	−6.8	−6.2	−6.0
Imd2	−8.2	−9.6	−9.2	−8.0

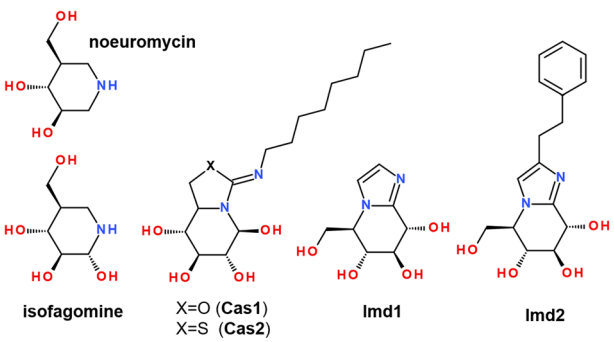

Scheme 3 Structure of the known inhibitors of enzymes from the β-glucosidase family.

examined by all-atom molecular dynamics (MD) simulations (Fig. 8A). MD simulations can provide detailed information about the conformational changes and fluctuations in a protein and a ligand.

The best-docked conformation of flavonols **2a–f** based on molecular docking was used as the initial conformation for MD sampling. The structural stability of the bound conformation of flavonol in its complex with the enzyme was evaluated by calculating the root mean square displacement (RMSD) over 200 ns. RMSD measures the deviation of a set of current coordinates of a molecule to a reference set of coordinates. RMSD time traces for the given flavonol were calculated by least-square fitting the ligand structure (τ_2) to its initially-docked structure ($\tau_1 = 0$) by eqn (5):

$$\mathrm{RMSD}(\tau_1,\ \tau_2) = \left[\frac{1}{N}\sum_{i=1}^{N}\|r_i(\tau_1) - r_i(\tau_2)\|^2\right]^{\frac{1}{2}} \quad (5)$$

where N and $r_i(\tau)$ are the number of atoms, and the position atom i and its reference position at time τ.[58,86]

The RMSD time traces for flavonols **2a–f** in its complex with β-glucosidase are shown in Fig. 8B. The analysis of these time traces demonstrates different mobility of the studied compounds within the ligand–protein complex; however, all

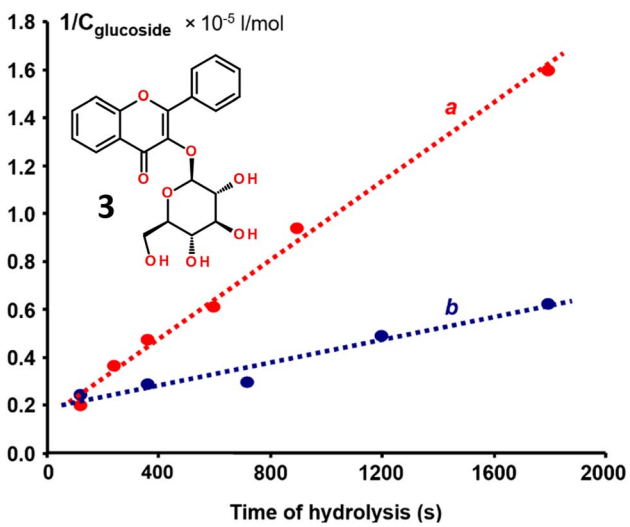

Fig. 7 The 2nd order kinetics plots for the enzymatic cleavage reaction of a fluorescent indicator, 3-hydroxyflavone glucoside **3** by β-glucosidase: (a) the free enzyme without any inhibitor and (b) the enzyme in the presence of flavonol **2e**.

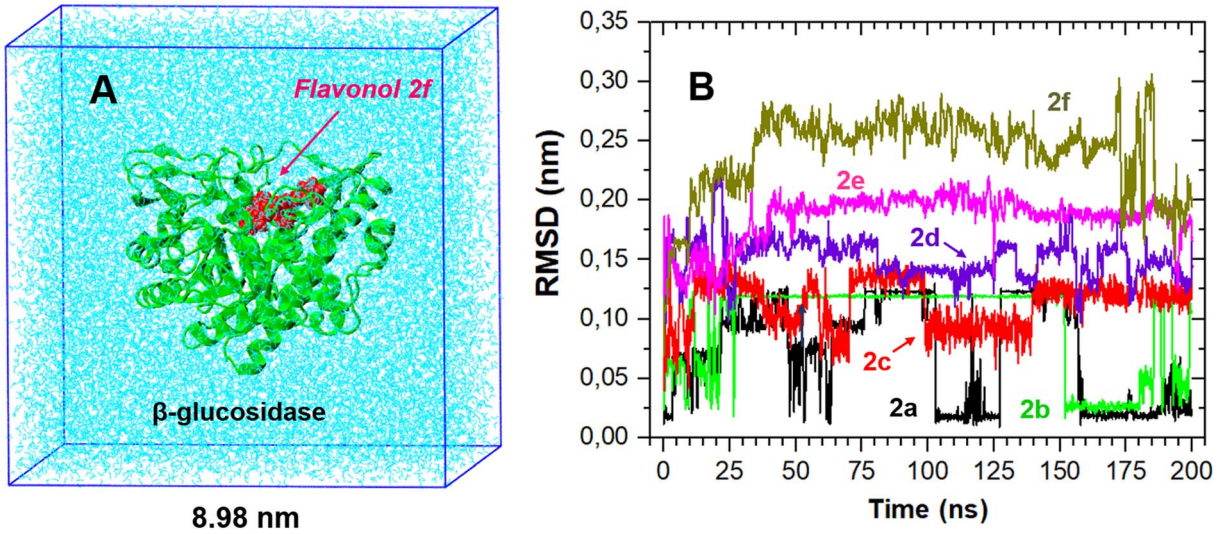

Fig. 8 (A) An example of MD simulations of the flavonol–enzyme complex for **2f** in explicit water solution. The initial structure of the complex was taken as the most favorable structure from the molecular docking calculations. (B) RMSD time traces of the coordinate positions of flavonols **2a–f** with the respect to their initial docked structure.

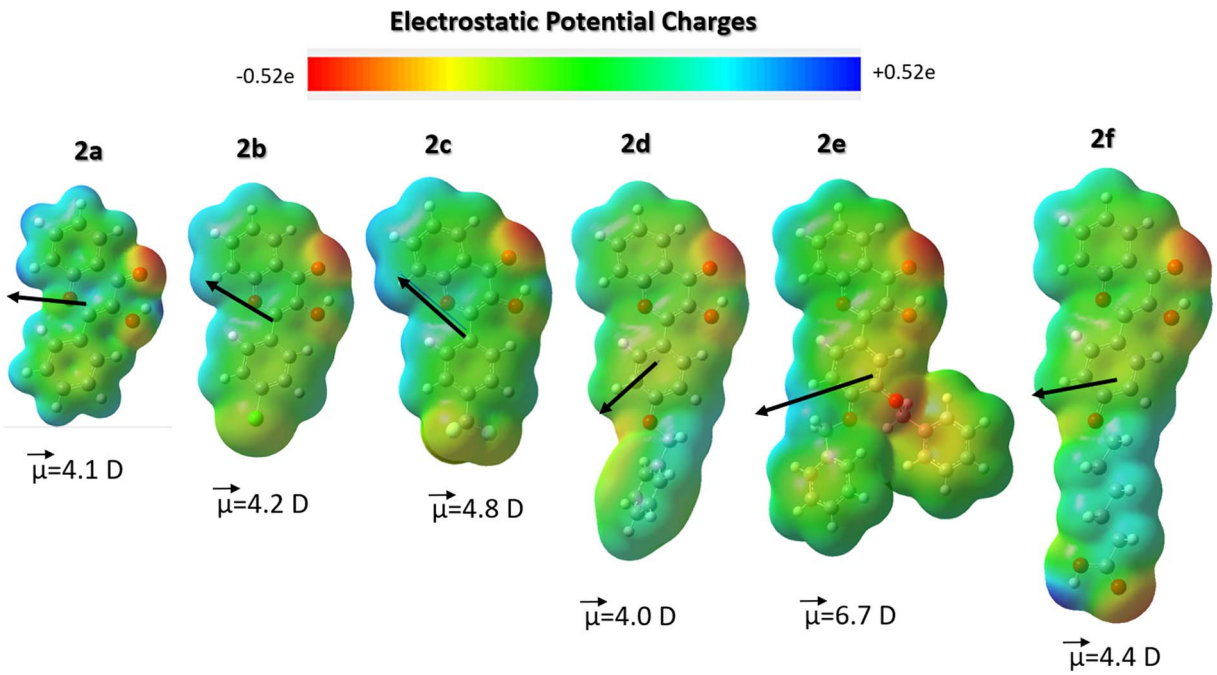

Fig. 9 Comparison of electrostatic potential (ESP) maps with an isosurface value of 0.010 e $Å^{-3}$, showing charge density distributions across flavonols **2a–f**. A ground-state dipole moment is shown as a vector and its absolute value is given in Debye (D). The DFT calculations were carried out at the B3LYP/cc-pVDZ level.

studied complexes remained stable during the MD sampling. The RMSD plots suggest that flavonols **2a–c** were located near their initial docked positions during all time. Flavonols **2d–f** revealed some high-amplitude mobility, which indicates some changes in their conformations and binding locations concerning the initially docked poses.

The above findings suggest that an energy balance between hydrophobic van-der-Waals and electrostatic interactions drove the observed strong binding of **2d–f** to β-glucosidases. Therefore, to examine the polar fragments and hydrophobic spots on the surface of the studied flavonols **2a–f**, we performed DFT calculations of their ground-state structure and electronic properties, as summarized in Fig. 9. The ESP maps demonstrate that flavonols **2a–f** have some polar regions near the carbonyl oxygen atoms of a chromone moiety. In contrast, most surface areas of probes have a relatively neutral hydrophobic character. These findings further support their strong hydrophobically-driven binding behavior towards the protein environment.

Summary and perspectives

In summary, we have synthesized a series of fluorescent flavonol derivatives **2a–f** containing different polar halogen-containing groups or bulky aromatic/alkyl substituents in the 2-aryl ring with the goal of tuning their hydrophobic/hydrophilic interactions with β-glucosidase enzyme. Using fluorescence titration experiments, we found that, upon adding almonds β-glucosidase, all studied flavonols revealed protein-induced fluorescence "turn-on" effects, which is indicative of their binding to the enzyme. The quantitative analysis of the binding isotherms demonstrated that flavonols **2e** and **2f** had the highest binding constants compared to unsubstituted or halogen-substituted derivatives **2a** and **2b**, which suggests that hydrophobic forces mostly drove the strong binding of **2e** and **2f** to β-glucosidase. In terms of the binding affinity, the studied flavonols belong to strong β-glucosidase binders, so they may also inhibit the enzyme activity. Indeed, using a fluorescent assay, we demonstrated that the binding of flavonol **2e** to β-glucosidase decreased its enzymatic activity up to 3.5 times.

Molecular aspects of flavonol–enzyme interactions were in-depth analyzed by molecular docking calculations, which demonstrate that the studied flavonols bind to the catalytic active site of β-glucosidase, so that they block and shield the key catalytic Glu residues of the enzyme from contacts with other substrate molecules. In addition, these calculations further support our suggestion that the substrate binding is governed by hydrophobic interactions with several aromatic Trp and Tyr residues within the catalytic glycone binding pockets of β-glucosidase. In addition, all-atom MD simulations of the docked conformations of flavonols **2a–f** in its complex with β-glucosidase in explicit water solution confirmed their high structural stability. Finally, we believe that our study provides a novel insight into structure–property relations for flavonol–protein interactions, which drives and governs their enzyme binding and outlines a framework for a rational design of new flavonol-based potent inhibitors for β-glucosidase enzymes.

Author contributions

Liudmyla V. Chepeleva: methodology, data, writing – original draft. Oleksii O. Demidov: data, resources, writing – original draft. Arsenii D. Snizhko: data, resources. Dmytro O. Tarasenko: data, resources. Andrii Y. Chumak: data, resources. Oleksii O. Kolomoitsev: methodology, resources, writing – original draft. Volodymyr M. Kotliar: conceptualization, methodology. Eugene S. Gladkov: methodology, writing – original draft. Alexander Kyrychenko: conceptualization, methodology, writing – review & editing. Alexander D. Roshal: conceptualization, writing – review & editing, supervision.

Conflicts of interest

There are no conflicts to declare.

Acknowledgements

D. O. T., O. O. K., A. Y. C., E. S. G., A. V. K., A. D. R. acknowledge Grant 2020.02/0016 (0121U112517) "Indicators based on chromone derivatives for fluorescent determination of β-glucosidase activity" from the National Research Foundation of Ukraine.

References

1 I. E. Serdiuk and A. D. Roshal, Exploring double proton transfer: a review on photochemical features of compounds with two proton-transfer sites, *Dyes Pigm.*, 2017, **138**, 223–244.
2 A. S. Klymchenko, Solvatochromic and Fluorogenic Dyes as Environment-Sensitive Probes: Design and Biological Applications, *Acc. Chem. Res.*, 2017, **50**, 366–375.
3 S. Höfener, P. C. Kooijman, J. Groen, F. Ariese and L. Visscher, Fluorescence behavior of (selected) flavonols: a combined experimental and computational study, *Phys. Chem. Chem. Phys.*, 2013, **15**, 12572–12581.
4 A. Y. Chumak, V. O. Mudrak, V. M. Kotlyar and A. O. Doroshenko, 4′-Nitroflavonol fluorescence: excited state intramolecular proton transfer reaction from the non-emissive excited state, *J. Photochem. Photobiol., A*, 2021, **406**, 112978.
5 Z. Xu, X. Zhao, M. Zhou, Z. Zhang, T. Qin, D. Wang, L. Wang, X. Peng and B. Liu, Donor engineering on flavonoid-based probes to enhance the fluorescence brightness in water: design, characterization, photophysical properties, and application for cysteine detection, *Sens. Actuators, B*, 2021, **345**, 130367.
6 T. Qin, B. Liu, Y. Huang, K. Yang, K. Zhu, Z. Luo, C. Pan and L. Wang, Ratiometric fluorescent monitoring of methanol in biodiesel by using an ESIPT-based flavonoid probe, *Sens. Actuators, B*, 2018, **277**, 484–491.
7 T. Qin, B. Liu, Z. Xu, G. Yao, H. Xu and C. Zhao, Flavonol-based small-molecule fluorescent probes, *Sens. Actuators, B*, 2021, **336**, 129718.
8 A. D. Roshal, J. A. Organero and A. Douhal, Tuning the mechanism of proton-transfer in a hydroxyflavone derivative, *Chem. Phys. Lett.*, 2003, **379**, 53–59.
9 I. E. Serdiuk and A. D. Roshal, Single and double intramolecular proton transfers in the electronically excited state of flavone derivatives, *RSC Adv.*, 2015, **5**, 102191–102203.
10 V. G. Pivovarenko, Multi-parametric sensing by multi-channel molecular fluorescent probes based on excited state intramolecular proton transfer and charge transfer processes, *BBA Adv.*, 2023, **3**, 100094.
11 A. O. Doroshenko, A. V. Kyrychenko, O. M. Valyashko, V. N. Kotlyar and D. A. Svechkarev, 4′-Methoxy-3-hydroxyflavone excited state intramolecular proton transfer reaction in alcoholic solutions: intermolecular versus intramolecular hydrogen bonding effect, *J. Photochem. Photobiol., A*, 2019, **383**, 111964.
12 A. P. Demchenko, S. Ercelen, A. D. Roshal and A. S. Klymchenko, Excited-State Proton Transfer Reaction

in a New Benzofuryl 3-Hydroxychromone Derivative: The Influence of Low-Polar Solvents, *Pol. J. Chem.*, 2002, **76**, 1287–1299.

13 V. F. Valuk, G. Duportail and V. G. Pivovarenko, A wide-range fluorescent pH-indicator based on 3-hydroxyflavone structure, *J. Photochem. Photobiol., A*, 2005, **175**, 226–231.

14 X. Poteau, G. Saroja, C. Spies and R. G. Brown, The photophysics of some 3-hydroxyflavone derivatives in the presence of protons, alkali metal and alkaline earth cations, *J. Photochem. Photobiol., A*, 2004, **162**, 431–439.

15 W. Liu, Y. Wang, W. Jin, G. Shen and R. Yu, Solvatochromogenic flavone dyes for the detection of water in acetone, *Anal. Chim. Acta*, 1999, **383**, 299–307.

16 D. Svechkarev, A. Kyrychenko, W. M. Payne and A. M. Mohs, Probing the self-assembly dynamics and internal structure of amphiphilic hyaluronic acid conjugates by fluorescence spectroscopy and molecular dynamics simulations, *Soft Matter*, 2018, **14**, 4762–4771.

17 B. Liu, Y. Pang, R. Bouhenni, E. Duah, S. Paruchuri and L. McDonald, A step toward simplified detection of serum albumin on SDS-PAGE using an environment-sensitive flavone sensor, *Chem. Commun.*, 2015, **51**, 11060–11063.

18 K. A. Bertman, C. S. Abeywickrama, H. J. Baumann, N. Alexander, L. McDonald, L. P. Shriver, M. Konopka and Y. Pang, A fluorescent flavonoid for lysosome detection in live cells under "wash free" conditions, *J. Mater. Chem. B*, 2018, **6**, 5050–5058.

19 X. Jin, X. Sun, X. Di, X. Zhang, H. Huang, J. Liu, P. Ji and H. Zhu, Novel fluorescent ESIPT probe based on flavone for nitroxyl in aqueous solution and serum, *Sens. Actuators, B*, 2016, **224**, 209–216.

20 K. A. Bertman, C. S. Abeywickrama, A. Ingle, L. P. Shriver, M. Konopka and Y. Pang, A Fluorescent Flavonoid for Lysosome Imaging: the Effect of Substituents on Selectivity and Optical Properties, *J. Fluoresc.*, 2019, **29**, 599–607.

21 I. E. Serdiuk, M. Reszka, A. Synak, B. Liberek and P. Bojarski, Determination of low-activity hydrolases using ESIPT fluorescent indicators on silver surfaces, *Dyes Pigm.*, 2018, **149**, 224–228.

22 S. Concilio, M. Di Martino, A. M. Nardiello, B. Panunzi, L. Sessa, Y. Miele, F. Rossi and S. Piotto, A Flavone-Based Solvatochromic Probe with a Low Expected Perturbation Impact on the Membrane Physical State, *Molecules*, 2020, **25**, 3458.

23 L. McDonald, B. Liu, A. Taraboletti, K. Whiddon, L. P. Shriver, M. Konopka, Q. Liu and Y. Pang, Fluorescent flavonoids for endoplasmic reticulum cell imaging, *J. Mater. Chem. B*, 2016, **4**, 7902–7908.

24 B. Liu, J. Wang, G. Zhang, R. Bai and Y. Pang, Flavone-Based ESIPT Ratiometric Chemodosimeter for Detection of Cysteine in Living Cells, *ACS Appl. Mater. Interfaces*, 2014, **6**, 4402–4407.

25 B. Liu, L. McDonald, Q. Liu, X. Bi, J. Zheng, L. Wang and Y. Pang, A flavonoid-based light-up bioprobe with intramolecular charge transfer characteristics for wash-free fluorescence imaging in vivo, *Sens. Actuators, B*, 2016, **235**, 309–315.

26 I. E. Serdiuk, M. Reszka, H. Myszka, K. Krzymiński, B. Liberek and A. D. Roshal, Flavonol-based fluorescent indicator for determination of β-glucosidase activity, *RSC Adv.*, 2016, **6**, 42532–42536.

27 M. Reszka, I. E. Serdiuk, K. Kozakiewicz, A. Nowacki, H. Myszka, P. Bojarski and B. Liberek, Influence of a 4′-substituent on the efficiency of flavonol-based fluorescent indicators of β-glycosidase activity, *Org. Biomol. Chem.*, 2020, **18**, 7635–7648.

28 A. T. Adetunji, F. B. Lewu, R. Mulidzi and B. Ncube, The biological activities of β-glucosidase, phosphatase and urease as soil quality indicators: a review, *J. Soil Plant Nutr.*, 2017, **17**, 794–807.

29 T. D. Butters, Gaucher disease, *Curr. Opin. Struct. Biol.*, 2007, **11**, 412–418.

30 X. Zhou, Z. Huang, H. Yang, Y. Jiang, W. Wei, Q. Li, Q. Mo and J. Liu, β-Glucosidase inhibition sensitizes breast cancer to chemotherapy, *Biomed. Pharmacother.*, 2017, **91**, 504–509.

31 U. Ghani, M. Nur-e-Alam, M. Yousaf, Z. Ul-Haq, O. M. Noman and A. J. Al-Rehaily, Natural flavonoid α-glucosidase inhibitors from Retama raetam: enzyme inhibition and molecular docking reveal important interactions with the enzyme active site, *Bioorg. Chem.*, 2019, **87**, 736–742.

32 S. P. Schröder, L. Wu, M. Artola, T. Hansen, W. A. Offen, M. J. Ferraz, K.-Y. Li, J. M. F. G. Aerts, G. A. van der Marel, J. D. C. Codée, G. J. Davies and H. S. Overkleeft, Gluco-1H-imidazole: A New Class of Azole-Type β-Glucosidase Inhibitor, *J. Am. Chem. Soc.*, 2018, **140**, 5045–5048.

33 P.-S. Tseng, C. Ande, K. W. Moremen and D. Crich, Influence of Side Chain Conformation on the Activity of Glycosidase Inhibitors, *Angew. Chem., Int. Ed.*, 2023, **62**, e202217809.

34 X. Liu, F. Li, L. Su, M. Wang, T. Jia, X. Xu, X. Li, C. Wei, C. Luo, S. Chen and H. Chen, Design and synthesis of novel benzimidazole-iminosugars linked a substituted phenyl group and their inhibitory activities against β-glucosidase, *Bioorg. Chem.*, 2022, **127**, 106016.

35 G. Legler, in *Advances in Carbohydrate Chemistry and Biochemistry*, ed. R. S. Tipson and D. Horton, Academic Press, 1990, vol. 48, pp. 319–384.

36 V. H. Lillelund, H. H. Jensen, X. Liang and M. Bols, Recent Developments of Transition-State Analogue Glycosidase Inhibitors of Non-Natural Product Origin, *Chem. Rev.*, 2002, **102**, 515–554.

37 A. K. Maurya, V. Mulpuru and N. Mishra, Discovery of Novel Coumarin Analogs against the α-Glucosidase Protein Target of Diabetes Mellitus: Pharmacophore-Based QSAR, Docking, and Molecular Dynamics Simulation Studies, *ACS Omega*, 2020, **5**, 32234–32249.

38 T. D. Heightman and A. T. Vasella, Recent Insights into Inhibition, Structure, and Mechanism of Configuration-Retaining Glycosidases, *Angew. Chem., Int. Ed.*, 1999, **38**, 750–770.

39 O. O. Demidov, E. S. Gladkov, A. V. Kyrychenko and A. D. Roshal, Synthetic and Natural Flavonols as Promising

Fluorescence Probes for β-Glucosidase Activity Screening, *Funct. Mater.*, 2022, **29**, 252–262.

40 S. H. White, W. C. Wimley, A. S. Ladokhin and K. Hristova, Protein folding in membranes: determining the energetics of peptide-bilayer interactions, *Methods Enzymol.*, 1998, **295**, 62–87.

41 T. Roy, S. T. Boateng, S. Banang-Mbeumi, P. K. Singh, P. Basnet, R.-C. N. Chamcheu, F. Ladu, I. Chauvin, V. S. Spiegelman, R. A. Hill, K. G. Kousoulas, B. M. Nagalo, A. L. Walker, J. Fotie, S. Murru, M. Sechi and J. C. Chamcheu, Synthesis, inverse docking-assisted identification and in vitro biological characterization of flavonol-based analogs of fisetin as c-Kit, CDK2 and mTOR inhibitors against melanoma and non-melanoma skin cancers, *Bioorg. Chem.*, 2021, **107**, 104595.

42 F. A. A. van Acker, J. A. Hageman, G. R. M. M. Haenen, W. J. F. van der Vijgh, A. Bast and W. M. P. B. Menge, Synthesis of Novel 3,7-Substituted-2-(3′,4′-dihydroxyphenyl) flavones with Improved Antioxidant Activity, *J. Med. Chem.*, 2000, **43**, 3752–3760.

43 Z. Qiang, W. Chun, L. Yunping and P. Wenchen, Synthesis and antibacterial activity of flavonols, *Chin. J. Appl. Environ. Biol.*, 2017, **23**, 232–237.

44 D. S. Goodsell, G. M. Morris and A. J. Olson, Automated docking of flexible ligands: applications of Autodock, *J. Mol. Recognit.*, 1996, **9**, 1–5.

45 O. Trott and A. J. Olson, AutoDock Vina: improving the speed and accuracy of docking with a new scoring function, efficient optimization, and multithreading, *J. Comput. Chem.*, 2010, **31**, 455–461.

46 P. Isorna, J. Polaina, L. Latorre-García, F. J. Cañada, B. González and J. Sanz-Aparicio, Crystal Structures of Paenibacillus polymyxa β-Glucosidase B Complexes Reveal the Molecular Basis of Substrate Specificity and Give New Insights into the Catalytic Machinery of Family I Glycosidases, *J. Mol. Biol.*, 2007, **371**, 1204–1218.

47 L. Xia, M. Ruppert, M. Wang, S. Panjikar, H. Lin, C. Rajendran, L. Barleben and J. Stöckigt, Structures of Alkaloid Biosynthetic Glucosidases Decode Substrate Specificity, *ACS Chem. Biol.*, 2012, **7**, 226–234.

48 D. L. Zechel, A. B. Boraston, T. Gloster, C. M. Boraston, J. M. Macdonald, D. M. G. Tilbrook, R. V. Stick and G. J. Davies, Iminosugar Glycosidase Inhibitors: Structural and Thermodynamic Dissection of the Binding of Isofagomine and 1-Deoxynojirimycin to β-Glucosidases, *J. Am. Chem. Soc.*, 2003, **125**, 14313–14323.

49 S. Tribolo, J.-G. Berrin, P. A. Kroon, M. Czjzek and N. Juge, The Crystal Structure of Human Cytosolic β-Glucosidase Unravels the Substrate Aglycone Specificity of a Family 1 Glycoside Hydrolase, *J. Mol. Biol.*, 2007, **370**, 964–975.

50 L. S. Dodda, I. Cabeza de Vaca, J. Tirado-Rives and W. L. Jorgensen, LigParGen web server: an automatic OPLS-AA parameter generator for organic ligands, *Nucleic Acids Res.*, 2017, **45**, W331–W336.

51 L. S. Dodda, J. Z. Vilseck, J. Tirado-Rives and W. L. Jorgensen, 1.14*CM1A-LBCC: Localized Bond-Charge Corrected CM1A Charges for Condensed-Phase Simulations, *J. Phys. Chem. B*, 2017, **121**, 3864–3870.

52 W. L. Jorgensen, D. S. Maxwell and J. Tirado-Rives, Development and Testing of the OPLS All-Atom Force Field on Conformational Energetics and Properties of Organic Liquids, *J. Am. Chem. Soc.*, 1996, **118**, 11225–11236.

53 W. L. Jorgensen, J. Chandrasekhar, J. D. Madura, R. W. Impey and M. L. Klein, Comparison of Simple Potential Functions for Simulating Liquid Water, *J. Chem. Phys.*, 1983, **79**, 926–935.

54 G. Bussi, D. Donadio and M. Parrinello, Canonical Sampling through Velocity Rescaling, *J. Chem. Phys.*, 2007, **126**, 014101.

55 T. Darden, D. York and L. Pedersen, Particle mesh Ewald: an N × log(N) method for Ewald sums in large systems, *J. Chem. Phys.*, 1993, **98**, 10089–10092.

56 B. Hess, H. Bekker, H. J. C. Berendsen and J. G. E. M. Fraaije, LINCS: A Linear Constraint Solver for Molecular Simulations, *J. Comput. Chem.*, 1997, **18**, 1463–1472.

57 B. Hess, P-LINCS: A Parallel Linear Constraint Solver for Molecular Simulation, *J. Chem. Theory Comput.*, 2008, **4**, 116–122.

58 D. Van Der Spoel, E. Lindahl, B. Hess, G. Groenhof, A. E. Mark and H. J. C. Berendsen, GROMACS: Fast, Flexible, and Free, *J. Comput. Chem.*, 2005, **26**, 1701–1718.

59 W. Humphrey, A. Dalke and K. Schulten, VMD: Visual Molecular Dynamics, *J. Mol. Graphics*, 1996, **14**, 33–38.

60 M. I. Lvovskaya, A. D. Roshal, A. O. Doroshenko, A. V. Kyrychenko and V. P. Khilya, Fluorescence behavior of chromones containing several protolytic centers. 3-Thiazolylchromones: emission band assignment and pH dependent effects, *Spectrochim. Acta, Part A*, 2006, **65**, 397–405.

61 L. Chebil, C. Humeau, J. Anthoni, F. Dehez, J.-M. Engasser and M. Ghoul, Solubility of Flavonoids in Organic Solvents, *J. Chem. Eng. Data*, 2007, **52**, 1552–1556.

62 W. Koenigs and E. Knorr, Ueber einige Derivate des Traubenzuckers und der Galactose, *Ber. Dtsch. Chem. Ges.*, 1901, **34**, 957–981.

63 D. W. Miller and K. A. Dill, Ligand binding to proteins: the binding landscape model, *Protein Sci.*, 1997, **6**, 2166–2179.

64 J. D. McGhee and P. H. von Hippel, Theoretical aspects of DNA-protein interactions: co-operative and non-co-operative binding of large ligands to a one-dimensional homogeneous lattice, *J. Mol. Biol.*, 1974, **86**, 469–489.

65 T. L. Hill, *Cooperativity Theory in Biochemistry: Steady-State and Equilibrium Systems*, Springer-Verlag, New York, Berlin, Heidelberg, Tokyo, 1985.

66 R. Gesztelyi, J. Zsuga, A. Kemeny-Beke, B. Varga, B. Juhasz and A. Tosaki, The Hill equation and the origin of quantitative pharmacology, *Archive for History of Exact Sciences*, 2012, **66**, 427–438.

67 S. Kuusk and P. Väljamäe, When substrate inhibits and inhibitor activates: implications of β-glucosidases, *Biotechnol. Biofuels*, 2017, **10**, 7.

68 C. He, X. Liu, Z. Jiang, S. Geng, H. Ma and B. Liu, Interaction Mechanism of Flavonoids and α-Glucosidase: Experimental and Molecular Modelling Studies, *Foods*, 2019, **8**, 355.
69 M. Fu, W. Shen, W. Gao, L. Namujia, X. Yang, J. Cao and L. Sun, Essential moieties of myricetins, quercetins and catechins for binding and inhibitory activity against α-Glucosidase, *Bioorg. Chem.*, 2021, **115**, 105235.
70 X. Ding, Y. Yu and Z. Ding, Interaction between active compounds from Rosa roxburghii Tratt and β-glucosidase: characterization of complexes and binding mechanism, *LWT*, 2022, **165**, 113707.
71 D. Liu, X. Cao, Y. Kong, T. Mu and J. Liu, Inhibitory mechanism of sinensetin on α-glucosidase and non-enzymatic glycation: insights from spectroscopy and molecular docking analyses, *Int. J. Biol. Macromol.*, 2021, **166**, 259–267.
72 Y. Bhatia, S. Mishra and V. S. Bisaria, Microbial β-Glucosidases: Cloning, Properties, and Applications, *Crit. Rev. Biotechnol.*, 2002, **22**, 375–407.
73 J. R. Ketudat Cairns, B. Mahong, S. Baiya and J.-S. Jeon, β-Glucosidases: multitasking, moonlighting or simply misunderstood?, *Plant Sci.*, 2015, **241**, 246–259.
74 S. He and S. G. Withers, Assignment of Sweet Almond β-Glucosidase as a Family 1 Glycosidase and Identification of Its Active Site Nucleophile, *J. Biol. Chem.*, 1997, **272**, 24864–24867.
75 A. D. Snizhko, A. V. Kyrychenko and E. S. Gladkov, Synthesis of Novel Derivatives of 5,6,7,8-Tetrahydro-quinazolines Using of α-Aminoamidines and In Silico Screening of Their Biological Activity, *Int. J. Mol. Sci.*, 2022, **23**, 3781.
76 G.-Y. Chen, H. Zhang and F.-Q. Yang, A simple and portable method for β-glucosidase activity assay and its inhibitor screening based on a personal glucose meter, *Anal. Chim. Acta*, 2021, **1142**, 19–27.
77 M. Kazmi, S. Zaib, A. Ibrar, S. T. Amjad, Z. Shafique, S. Mehsud, A. Saeed, J. Iqbal and I. Khan, A new entry into the portfolio of α-glucosidase inhibitors as potent therapeutics for type 2 diabetes: design, bioevaluation and one-pot multi-component synthesis of diamine-bridged coumarinyl oxadiazole conjugates, *Bioorg. Chem.*, 2018, **77**, 190–202.
78 S. Riaz, I. U. Khan, M. Yar, M. Ashraf, T. U. Rehman, A. Shaukat, S. B. Jamal, V. C. M. Duarte and M. J. Alves, Novel pyridine-2,4,6-tricarbohydrazide derivatives: design, synthesis, characterization and in vitro biological evaluation as α- and β-glucosidase inhibitors, *Bioorg. Chem.*, 2014, **57**, 148–154.
79 S. Khan, T. Pozzo, M. Megyeri, S. Lindahl, A. Sundin, C. Turner and E. N. Karlsson, Aglycone specificity of Thermotoga neapolitana β-glucosidase 1A modified by mutagenesis, leading to increased catalytic efficiency in quercetin-3-glucoside hydrolysis, *BMC Biochem.*, 2011, **12**, 11.
80 C. Proença, M. Freitas, D. Ribeiro, E. F. T. Oliveira, J. L. C. Sousa, S. M. Tomé, M. J. Ramos, A. M. S. Silva, P. A. Fernandes and E. Fernandes, α-Glucosidase inhibition by flavonoids: an in vitro and in silico structure–activity relationship study, *J. Enzyme Inhib. Med. Chem.*, 2017, **32**, 1216–1228.
81 L. Zeng, G. Zhang, S. Lin and D. Gong, Inhibitory Mechanism of Apigenin on α-Glucosidase and Synergy Analysis of Flavonoids, *J. Agric. Food Chem.*, 2016, **64**, 6939–6949.
82 K. Tadera, Y. Minami, K. Takamatsu and T. Matsuoka, Inhibition of α-Glucosidase and α-Amylase by Flavonoids, *J. Nutr. Sci. Vitaminol.*, 2006, **52**, 149–153.
83 S. Horikoshi, W. Saburi, J. Yu, H. Matsuura, J. R. K. Cairns, M. Yao and H. Mori, Substrate specificity of glycoside hydrolase family 1 β-glucosidase AtBGlu42 from Arabidopsis thaliana and its molecular mechanism, *Biosci., Biotechnol., Biochem.*, 2021, **86**, 231–245.
84 R. Uehara, R. Iwamoto, S. Aoki, T. Yoshizawa, K. Takano, H. Matsumura and S.-i. Tanaka, Crystal structure of a GH1 β-glucosidase from Hamamotoa singularis, *Protein Sci.*, 2020, **29**, 2000–2008.
85 T. M. Gloster, S. Roberts, G. Perugino, M. Rossi, M. Moracci, N. Panday, M. Terinek, A. Vasella and G. J. Davies, Structural, Kinetic, and Thermodynamic Analysis of Glucoimidazole-Derived Glycosidase Inhibitors, *Biochemistry*, 2006, **45**, 11879–11884.
86 D. Van Der Spoel, E. Lindahl, B. Hess, A. R. van Buuren, E. Apol, P. J. Meulenhoff, D. P. Tieleman, A. L. T. M. Sijbers, K. A. Feenstra, R. van Drunen and H. J. C. Berendsen, *Gromacs User Manual Version 4.5.4*, 2010, **https://www.gromacs.org/**.